

Investigation of the Gamma-Ray Bursts prompt emission under the relativistically expanding fireball scenario

SOUMYA GUPTA^{*1,2} AND SUNDER SAHAYANATHAN^{+1,2}

¹*Homi Bhabha National Institute, Mumbai, Maharashtra, India*

²*Bhabha Atomic Research Center, Mumbai, Maharashtra, India*

ABSTRACT

The spectral properties of a composite thermal emission arising from a relativistic expanding fireball can be remarkably different from the Planck function. We perform a detailed study of such a system to explore the features of the prompt emission spectra from the gamma-ray bursts (GRBs). Particularly, we address the effect of optical opacity and its dependence on the density profile between the expanding gas and the observer. This results in a nontrivial shape of the photospheric radius which in combination with the constraints derived from the equal-arrival-time can result in a mild broader spectrum compared to the Planck function. Further, we show the time-integrated spectrum from the expanding fireball deviates significantly from the instantaneous emission and is capable of explaining the observed broad spectral width of the GRBs. We also show, that the demand of the spectral width of the order of unity, obtained through statistical analysis, is consistent with the scenario where the dynamics of the expanding fireball are governed predominantly by the energy content of the matter.

Keywords: Gamma-ray bursts–X-ray transient sources–Radiative processes

1. INTRODUCTION

Gamma-Ray Bursts (GRB) are the brightest events that spate the radiation in a brief duration of time. They carry tremendous energy lasting from a few ms to a hundred seconds, which outshines any sources in the sky. This short-lived burst of radiation, bright in γ -ray and hard X-ray, is referred to as the prompt phase of GRB. Even after decades of study using several space-based missions, the radiation mechanism of the prompt phase is still under debate (Rees & Mészáros 2005; Pe'er 2008; Beloborodov 2011; Zhang et al. 2014). Among various models, the competitive ones are the decoupled thermal emission associated with the expansion of an initial optically thick fireball (Cavallo & Rees 1978; Paczynski 1986; Goodman 1986; Shemi & Piran 1990; Piran et al. 1993) and the non-thermal origin due to synchrotron loss from an electron distribution accelerated at the shock fronts (Rees & Meszaros 1994; Tavani 1996; Cohen & Piran 1997; Sari & Piran 1997; Bošnjak et al. 2009; Daigne et al. 2011; Zhang & Yan 2011). Nevertheless, under the fireball scenario, both these emission products are viable since after the release of the initial thermal energy, the matter coasts relativistically

developing shocks which dissipate the bulk energy of the flow (Thompson 1994; Ghisellini & Celotti 1999; Lazzati & Begelman 2010; Lazzati et al. 2011; Beloborodov 2012).

The dynamics of an expanding fireball are mainly governed by the factor η , the ratio of the energy content in radiation E_0 to the total rest mass energy of the matter M_0c^2 at the beginning of the burst (Shemi & Piran 1990; Piran et al. 1993). In the initial phase of evolution, the fireball is optically thick and expands freely at the expense of its internal energy ($\eta \gg 1$), with the bulk Lorentz factor (Γ) of the flow proportional to the radius ($\Gamma \sim R$) (Goodman 1986). The temperature of the fireball at this phase will largely remain constant. The acceleration phase continues till $\eta \sim 1$ and from there on, the energy content of the matter dominates the evolution of the fireball. During this matter-dominant phase ($\eta \ll 1$), the fireball coasts with a constant bulk velocity and the temperature scales as $R^{-2/3}$ (Piran et al. 1993).

In the course of evolution, the temperature of the fireball drops and once it falls below the pair production threshold, the radiation decouples from the matter, releasing a burst of radiation. The radius of the fireball where the last scattering surface of the trapped photons falls is referred to as photospheric radius R_{ph} . Interestingly, R_{ph} can fall either during $\eta > 1$ or $\eta < 1$ phase and the observed burst property will vary significantly under these two scenarios. When $\eta > 1$, the matter is still in the accelerating phase and the instantaneous Doppler boosting nullifies the adiabatic loss. Hence,

Corresponding author: Soumya Gupta, Sunder Sahayanathan
soumya.gupta1512@gmail.com/soumyag@barc.gov.in,
sunder@barc.gov.in

the observed burst luminosity will be equal to that of the initial outflow (Mészáros & Rees 2000). On the other hand, when $\eta < 1$, the flow incurs significant adiabatic loss and the observed burst luminosity will be less than the initial outflow.

The effect of the viewing angle and the relativistic flow have a substantial role in the observed shape of the photospheric surface of the burst. For a spherically symmetric expanding matter, the photospheric radius measured by a distant observer $R_{ph}(\theta)$ will be larger for the higher viewing angle (high latitude) of the emission cone. This will result in a non-trivial concave shape of the photospheric surface (§2.1)(Pe'er (2008), Meng et al. (2018)). Similarly, due to the relativistic expansion, the observed instantaneous emission released from a certain radius has to travel a long distance in case of higher latitude compared to the on-axis emission. Hence, the surface constructed from the photons reaching the observer at the same time (*equal-time-surface*) will deviate from a spherical shape. If the expansion is associated with a fall in the temperature of the fireball, then the *equal-time-surface* will be a superposition of multiple temperatures. These effects will significantly modify the initial observed emission profile and the spectrum of the GRB prompt phase (§2.2).

Irrespective of the radiative model, the prompt emission of GRBs is often well represented by an empirical function involving a broken power-law with an exponential turnover, commonly referred to as the Band function (Band et al. 1993). This function is useful to identify the peak frequency, the low energy and the high energy spectral indices which can be readily compared with the constraints derived from the radiative models (Preece et al. 2002; Pe'er & Zhang 2006; Uhm & Zhang 2014). Besides these, it also helps to understand the statistical property of a large sample of GRBs, for example, the correlation between the peak energy and the isotropic luminosity (Amati et al. 2002; Yonetoku et al. 2004; Liang et al. 2010). Another study involving a large sample of GRBs is their spectral width (FWHM: \mathcal{W}) distribution derived from the best-fit Band function parameters. For long GRBs the most probable \mathcal{W} is found to be ~ 1.07 estimated from a sample of 1873 GRBs and in the case of short GRBs, it was ~ 0.86 obtained from a sample of 419 GRBs (Axelsson & Borgonovo 2015). Interestingly, these widths are much broader than that of a Planck function (FWHM ≈ 0.54) while much narrower than a typical synchrotron spectrum (FWHM ~ 1.6).

In an attempt to explain the unusual \mathcal{W} of GRBs, Bharali et al. (2017) considered a multi-temperature blackbody spectrum associated with an evolving fireball. Nevertheless, the \mathcal{W} of ~ 1 demanded an unphysical faster rate of temperature evolution and this disfavoured the fireball interpretation of GRB prompt emission. In this work, we revisit the expanding fireball scenario of GRB prompt emission and show that a proper inclusion of the radial evolution is capable of explaining the observed \mathcal{W} of GRBs. The effect of the concave

photospheric surface and the emission cone limited by the relativistic effects are also considered in studying the temporal evolution of the fireball blackbody spectrum.

2. EXPANDING FIREBALL

2.1. Evolutionary Phase

The optical depth of a relativistically expanding spherical symmetric wind measured for a photon propagating towards an observer will be (Abramowicz et al. 1991)

$$\tau(r, \theta) = \frac{r_d}{\pi r} (\theta - \beta \sin \theta) \quad (1)$$

where, r is projected distance and θ is the angle with respect to the line of sight such that $r \sin \theta$ is the radial distance R of the emitted photon from the centre of the spherical wind. The quantity β is the velocity of expansion of the wind, assumed to be constant and expressed in the units of c , and r_d is the radius of the opaque disk measured by the observer for photons emerging from infinity. The observed photospheric radius will then be (Pe'er 2008)

$$R_{ph}(\theta) = \frac{R_{ph0}}{(1 - \beta)} \left(\frac{\theta}{\sin \theta} - \beta \right) \quad (2)$$

where, $R_{ph0} \approx r_d/2\pi\Gamma^2$ is the minimum photospheric radius measured at $\theta = 0$ and Γ is the bulk Lorentz factor of the plasma. Interestingly, R_{ph} will be an increasing function of θ and hence, the observer will visualize the photospheric surface as concave though the expansion is spherically symmetric (Figure 1).

Due to spherical expansion, the photons emitted on-axis will arrive earlier than those emitted at higher latitudes. Hence, the photons received by an observer at an instant will be a combination of higher latitude emissions, when the expanding plasma is young relative to the on-axis emission. The evolutionary *equal-time-surface* corresponding to the instantaneous emission by the observer can then be obtained as (Bharali et al. 2017)

$$R(\theta) = R(0) \left(\frac{1 - \beta}{1 - \beta \cos \theta} \right) \quad (3)$$

which is a decreasing function of θ and will be an ellipsoidal surface (Figure 1). Due to relativistic expansion, the emitted photons will be confined within a cone of a semi-vertical angle $1/\Gamma$. Hence, this angle limits the maximum higher latitude emission received by the observer with $R(\theta)|_{\max} \approx R(0)/(1 + \beta)$.

During the initial stage of evolution, the opening angle can be significantly smaller than $1/\Gamma$ and will be governed by $R_{ph}(\theta)$. Since $R(\theta) \geq R_{ph}(\theta)$ and from equations 2 and 3 we obtain

$$\frac{r_d}{\pi R(0)(1 - \beta)} \left(\frac{\theta}{\sin \theta} - \beta \right) (1 - \beta \cos \theta) \leq 1 \quad (4)$$

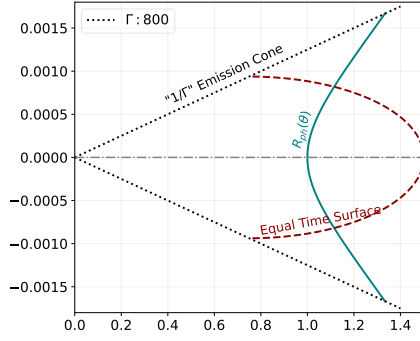


Figure 1. The plot depicts the *equal-time-surface* in red-dashed line, photospheric radius $R_{ph}(\theta)$ in teal-solid line and emission cone of angle $1/\Gamma$ in black-dotted line for the Γ of 800. The R_{ph0} is scaled to unity and the grey-dot-dashed line is the axis for $\theta = 0$.

For a given $R(0)$, the opening angle of the emission cone can be obtained by solving the above transcendental equation which will be smaller than $1/\Gamma$. The on-axis radial distance beyond which the angle of the emission cone will be constant at $1/\Gamma$ will be $R(0) \gtrsim (1 + \beta)R_{ph0}$.

As the fireball expands beyond $R_{ph}(\theta)$, the photons decouple from the inner regions and have a finite probability to be scattered along the line of sight (Pe'er 2008; Pe'er & Ryde 2011; Beloborodov 2011). The observed intensity of the radiation will then be proportional to

$$\zeta(\theta) = \int_{R_{in}}^{R(\theta)} \exp[-\tau(z, \theta)] dz \quad (5)$$

where, the direction of z is along the line of sight and $R_{in} = \text{MIN}\{[R(\theta) - R_{ph}(\theta)], R_{ph0} \cos(\theta)\}$. Using equations 1 and 2, we obtain

$$\zeta(\theta) = \int_{R_{in}}^{R(\theta)} \exp\left[\frac{-\cos(\theta) R_{ph}(\theta)}{z}\right] dz \quad (6)$$

The observed temperature of the fireball evolves depending on the energetics of the burst phase. In the radiation dominated phase ($\eta \gg 1$), $T_{\text{obs}} \sim \text{constant}$; while, in the matter dominated phase ($\eta \ll 1$), $T_{\text{obs}} \propto R^{-2/3}$. If we represent the on-axis temperature of the fireball as T_0 , then the temperature gradient observed over the *equal-time-surface* will be

$$\begin{aligned} \frac{T_\theta}{T_0} &= \left[\frac{R(0)}{R(\theta)}\right]^\alpha \\ &= \left(\frac{1 - \beta \cos \theta}{1 - \beta}\right)^\alpha \end{aligned} \quad (7)$$

where, α varies from 0 to $2/3$. In terms of the on-axis photospheric temperature T_{ph0} , the temperature gradient can be

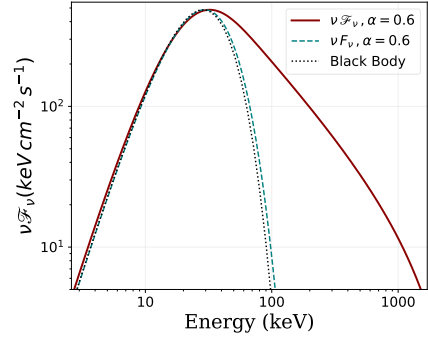


Figure 2. The plot represents the spectrum ($\alpha = 0.6$) for the time-averaged case ($\nu \mathcal{F}_\nu$) in a red-solid line, the instantaneous case (νF_ν) in a teal-dashed line and the black body in a black-dotted line.

expressed as

$$\frac{T_\theta}{T_{ph0}} = \left(\frac{R_{ph0}}{R(0)} \frac{1 - \beta \cos \theta}{1 - \beta}\right)^\alpha \quad (8)$$

2.2. Observed spectrum

The instantaneous flux from the expanding fireball measured by an observer located at a distance D_L will be

$$\begin{aligned} F_\nu &= \frac{2\pi}{D_L^2} \int_{\cos \phi}^1 I_\theta(\nu) R(\theta)^2 \zeta(\theta) \mu d\mu \\ &= \frac{2\pi R(0)^2 (1 - \beta)^2}{D_L^2} \int_{\cos \phi}^1 \frac{I_\theta(\nu)}{(1 - \beta \mu)^2} \zeta(\theta) \mu d\mu \end{aligned} \quad (9)$$

where, $I_\theta(\nu)$ is the observed specific intensity and $\mu = \cos \theta$. Using Lorentz invariance, $I_\theta(\nu)$ can be expressed in terms of the expanding gas comoving specific intensity $I'_\theta(\nu')$ as ¹

$$\begin{aligned} I_\theta(\nu) &= I'_\theta(\nu') \left(\frac{\nu}{\nu'}\right)^3 \\ &= \frac{2h}{c} \frac{\nu^3}{\exp\left(\frac{h\nu}{kT_\theta}\right) - 1} \end{aligned} \quad (10)$$

and using equations 6, 9 and 10, the observed instantaneous flux will be

$$\begin{aligned} F_\nu &= 4\pi h \nu^3 \left[\frac{(1 - \beta)R(0)}{c D_L}\right]^2 \times \\ &\int_{\cos \phi}^1 \frac{\mu}{(1 - \beta \mu)^2} \frac{\zeta(\theta) d\mu}{\left\{\exp\left[\frac{h\nu}{k T_{ph0}} \left(\frac{R(0)}{R_{ph0}} \frac{1 - \beta}{1 - \beta \mu}\right)^\alpha\right] - 1\right\}} \end{aligned} \quad (11)$$

¹ All the quantities represented with ' are measured in the expanding gas comoving frame.

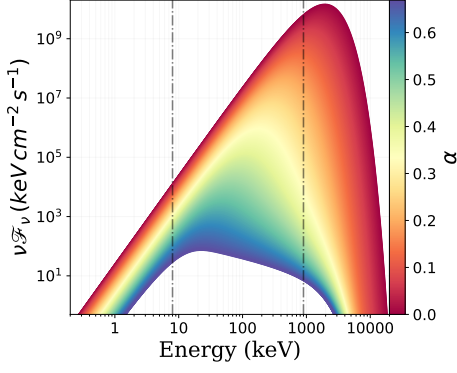


Figure 3. The plot represents the change in the time-integrated spectrum for the α ranging from 0 to $2/3$, color-mapped on the right axis. The vertical grey-dashed line represents the energy range of the NaI detector of the Gamma-Ray Burst Monitor (GBM) onboard *Fermi*.

In Figure 2, we show the instantaneous spectrum from the fireball along with an equivalent Planck function for α ranging from 0 to $2/3$. The temperature variation will be more pronounced for the time-averaged spectrum and will significantly deviate from the Planck function. Let us assume the evolution of the fireball for a duration Δt during which the on-axis radius expands from R_1 to $R_2 (= R_1 + 2\beta c\Gamma^2\Delta t)$. The time-averaged spectrum during Δt will be equivalent to

$$\mathcal{F}_\nu = \frac{\int_{R_1}^{R_2} F_\nu(x) dx}{R_2 - R_1} \quad (12)$$

In Figure 2, we show the time-averaged spectrum for a duration of 5s along with the Planck function. The spectral shape has a strong dependence on α (in Figure 3) and in Figure 4, we show the variation in the peak of the spectrum with respect to various model parameters. To study the variation in the spectrum due to an individual parameter, the rest of the parameters were fixed at $\Gamma = 100$, $R_{ph0} = 12.0 \log \text{ cm}$, $T_{ph0} = 500 \text{ keV}$, duration of burst $\Delta t = 5.0 \text{ sec}$ and $\alpha = 0.67$ (Figure 3, 4 and 5). We note the flux at the spectral peak enhances nearly by an order of ten (in Figure 3), when α is varied from 0 to $2/3$. However, the dynamic range of the detector will typically be of the order of 2-3. Therefore, the range of α that could be studied by an instrument will be $\Delta\alpha \sim 0.15$.

2.3. Spectral width

The time-averaged spectrum from the fireball can imitate various spectral shapes with the proper choice of α . Accordingly, their spectral width at half the maximum flux (\mathcal{W} , defined as $\mathcal{W} = \log(\nu_2/\nu_1)$), can vary with α . Besides this, the variation in other parameters may also impact \mathcal{W} . To investigate this, we estimated \mathcal{W} for a wide range of model parameters and the results are shown in Figure 4. It is evident the variation in \mathcal{W} is not prominent in the case of the

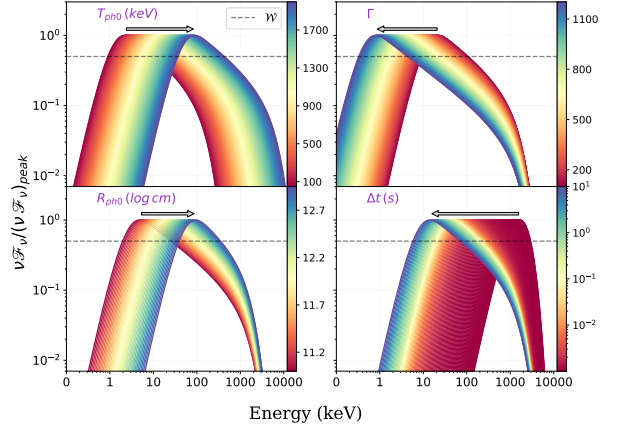


Figure 4. The plot exhibits the evolution of the time-integrated spectrum with different parameter space. The variation with T_{ph0} , Γ , R_{ph0} and Δt are plotted in the top-left, top-right, bottom-left and bottom-right panels respectively, and color-mapped on the right axis of each panel. The grey-dashed line is the spectral width. The spectrum is scaled with the value at peak energy to illustrate the shift in peak energy (direction of the arrow) with an increase in model parameters.

parameters Γ , R_{ph0} , Δt and T_{ph0} (The flux at half maximum is shown as a grey-dashed line in Figure 4). However, significant change in \mathcal{W} can be witnessed even with moderate variation in α .

The \mathcal{W} of the order of unity, supported by the observations (Axelsson & Borgonovo 2015), can be obtained only for the case when $\alpha \sim 0.65$ (which is close to $2/3$) and shown as yellow triangle in the top-left panel of Figure 5. Interestingly, besides providing an explanation for the observed spectral width of GRBs, these results also suggest that most of the radiation from the GRB is released during the matter-dominated phase of the expanding fireball.

3. DISCUSSION AND SUMMARY

The prominence of thermal emission in the GRB prompt phase has been well-studied by various authors (Ryde 2004, 2005; Pe'er 2008; Lundman et al. 2013; Pe'er & Ryde 2011) and often supported by observations such as GRB 100724B: (Guiriec et al. 2013), GRB 101219B: (Ghirlanda et al. 2013), GRB 081221: (Hou et al. 2018), GRB 220426A: (Wang et al. 2022). Nevertheless, the prompt emission also carries a significant contribution of non-thermal spectral component (Pe'er et al. 2012; Iyyani et al. 2013; Zhang et al. 2016; Wang et al. 2023). The evolution of the fireball during its coasting phase can deviate the spectral shape of the photospheric thermal emission from the Planck function. In this work, we show the spectral shape and the peak of the emission from a relativistically expanding fireball are primarily governed by four quantities namely, R_{ph0} , T_{ph0} , Γ and α (§2.2). Besides these, the integration time of the dynamically evolving fireball can extend the low energy end of the modified thermal emission.

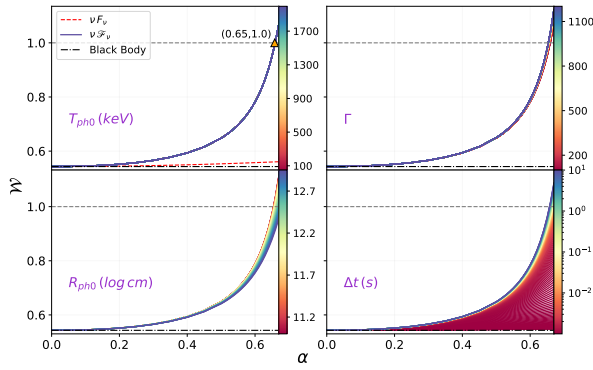


Figure 5. The plot represents the variation of \mathcal{W} of time-averaged spectra ($\nu \mathcal{F}_\nu$) with α , for different parameter space. The variation with T_{ph0} , Γ , R_{ph0} and Δt are plotted in the top-left, top-right, bottom-left and bottom-right panels respectively, and color-mapped on the right axis of each panel. The black-dot-dashed line corresponds to \mathcal{W} of the black body spectrum. In the first panel, the red-dashed line corresponds to \mathcal{W} of the instantaneous (νF_ν) spectrum.

The modified thermal emission obtained from an evolving fireball has a strong dependence on the index α . For lower values of α (~ 0.1), the spectrum peaks at the high energy corresponding to the photospheric temperature. On the other hand, for high values of α (≥ 0.4), it will be governed by the cooled photon temperature encountered during its evolution (Figure 3). This feature leads to a broad range of spectral widths starting from ~ 0.54 (nearly equal to that of the Planck function) to ~ 1.15 . Consistently, the observed \mathcal{W} can be extrapolated to infer the energetics of the burst ($\eta \ll 1$) (Piran et al. 1993; Axelsson & Borgonovo 2015). The model can also be applied to individual bursts to estimate the contribution of the thermal component and can probe the energetics of the burst.

The choice of other parameters R_{ph0} , T_{ph0} and Γ will affect only in shifting the spectral peak but have minimal impact on the spectral width (Figure 4 and 5). For a given α (≥ 0.2), the \mathcal{W} will increase with Δt only till a certain value. Beyond this, the evolution will modify the flux below the half

maximum and hence \mathcal{W} will remain constant (In bottom-right panel, figure 5). Axelsson & Borgonovo (2015) showed that the distribution of \mathcal{W} for a large sample of GRBs, suggests the most probable width to be ~ 1 . Incidentally, this width closely matches the width of the single particle emissivity of the synchrotron process. Hence, the authors concluded the GRBs with $\mathcal{W} \lesssim 1$ to be dominated by the synchrotron process; while the ones with $\mathcal{W} \gtrsim 1$ should be consistent with the modified thermal process. However, Burgess (2019) showed the synchrotron process itself is capable to explain many GRBs irrespective of their \mathcal{W} estimated from the Band function. In our work, we show that the modified thermal spectrum obtained from the evolving fireball is capable of explaining the spectral widths over the range $0.54 \lesssim \mathcal{W} \lesssim 1.2$.

If the decoupling of photons happens well within the radiation-dominated phase ($\eta > 1$), the temperature remains nearly constant whereas Γ increases with the evolving radius of the fireball. This scenario is not considered in the present work and has the potential to produce a spectrum which differs from the Planck function. Though the temperature remains constant, the enhancement in Γ will shift the emission to high energies resulting in a modified thermal spectrum. Interestingly, the evolved photon temperatures measured by the observer will be hotter than the photospheric temperature in such a case. A detailed study under this scenario will be presented elsewhere. In this work, we have considered only the thermal contribution of the fireball. Besides this, the burst spectra may involve the non-thermal emission arising from the shock accelerated particle distribution. The later contribution is evident from the observed polarisation of the GRBs (Chattopadhyay et al. 2021; Kole et al. 2020). Nevertheless, the observed peak spectral width suggests the thermal origin to be the dominant emission process.

The authors acknowledge the referee for the valuable suggestions. The authors also like to thank Dipankar Bhattacharya and A.R. Rao for the insightful discussions.

REFERENCES

- Abramowicz, M. A., Novikov, I. D., & Paczynski, B. 1991, *ApJ*, 369, 175, doi: [10.1086/169748](https://doi.org/10.1086/169748)
- Amati, L., Frontera, F., Tavani, M., et al. 2002, *A&A*, 390, 81, doi: [10.1051/0004-6361:20020722](https://doi.org/10.1051/0004-6361:20020722)
- Axelsson, M., & Borgonovo, L. 2015, *MNRAS*, 447, 3150, doi: [10.1093/mnras/stu2675](https://doi.org/10.1093/mnras/stu2675)
- Band, D., Matteson, J., Ford, L., et al. 1993, *ApJ*, 413, 281, doi: [10.1086/172995](https://doi.org/10.1086/172995)
- Beloborodov, A. M. 2011, *ApJ*, 737, 68, doi: [10.1088/0004-637X/737/2/68](https://doi.org/10.1088/0004-637X/737/2/68)
- Beloborodov, A. M. 2012, *The Astrophysical Journal*, 762, 13, doi: [10.1088/0004-637x/762/1/13](https://doi.org/10.1088/0004-637x/762/1/13)
- Bharali, P., Sahayanathan, S., Misra, R., & Boruah, K. 2017, *NewA*, 55, 22, doi: [10.1016/j.newast.2017.02.004](https://doi.org/10.1016/j.newast.2017.02.004)
- Bošnjak, Ž., Daigne, F., & Dubus, G. 2009, *A&A*, 498, 677, doi: [10.1051/0004-6361/200811375](https://doi.org/10.1051/0004-6361/200811375)
- Burgess, J. M. 2019, *A&A*, 629, A69, doi: [10.1051/0004-6361/201935140](https://doi.org/10.1051/0004-6361/201935140)
- Cavallo, G., & Rees, M. J. 1978, *MNRAS*, 183, 359, doi: [10.1093/mnras/183.3.359](https://doi.org/10.1093/mnras/183.3.359)

- Chattopadhyay, T., Gupta, S., Gupta, S., et al. 2021, *Journal of Astrrophysics and Astronomy*, 42, 20, doi: [10.1007/s12036-021-09718-2](https://doi.org/10.1007/s12036-021-09718-2)
- Cohen, E., & Piran, T. 1997, *ApJL*, 488, L7, doi: [10.1086/310916](https://doi.org/10.1086/310916)
- Daigne, F., Bošnjak, Ž., & Dubus, G. 2011, *A&A*, 526, A110, doi: [10.1051/0004-6361/201015457](https://doi.org/10.1051/0004-6361/201015457)
- Ghirlanda, G., Pescalli, A., & Ghisellini, G. 2013, *MNRAS*, 432, 3237, doi: [10.1093/mnras/stt681](https://doi.org/10.1093/mnras/stt681)
- Ghisellini, G., & Celotti, A. 1999, *ApJL*, 511, L93, doi: [10.1086/311845](https://doi.org/10.1086/311845)
- Goodman, J. 1986, *ApJL*, 308, L47, doi: [10.1086/184741](https://doi.org/10.1086/184741)
- Guiriec, S., Daigne, F., Hascoët, R., et al. 2013, *ApJ*, 770, 32, doi: [10.1088/0004-637X/770/1/32](https://doi.org/10.1088/0004-637X/770/1/32)
- Hou, S.-J., Zhang, B.-B., Meng, Y.-Z., et al. 2018, *ApJ*, 866, 13, doi: [10.3847/1538-4357/aadc07](https://doi.org/10.3847/1538-4357/aadc07)
- Iyyani, S., Ryde, F., Axelsson, M., et al. 2013, *MNRAS*, 433, 2739, doi: [10.1093/mnras/stt863](https://doi.org/10.1093/mnras/stt863)
- Kole, M., De Angelis, N., Berlato, F., et al. 2020, *Astronomy and Astrophysics*, 644, A124, doi: [10.1051/0004-6361/202037915](https://doi.org/10.1051/0004-6361/202037915)
- Lazzati, D., & Begelman, M. C. 2010, *ApJ*, 725, 1137, doi: [10.1088/0004-637X/725/1/1137](https://doi.org/10.1088/0004-637X/725/1/1137)
- Lazzati, D., Morsony, B. J., & Begelman, M. C. 2011, *ApJ*, 732, 34, doi: [10.1088/0004-637X/732/1/34](https://doi.org/10.1088/0004-637X/732/1/34)
- Liang, E.-W., Yi, S.-X., Zhang, J., et al. 2010, *ApJ*, 725, 2209, doi: [10.1088/0004-637X/725/2/2209](https://doi.org/10.1088/0004-637X/725/2/2209)
- Lundman, C., Pe'er, A., & Ryde, F. 2013, *MNRAS*, 428, 2430, doi: [10.1093/mnras/sts219](https://doi.org/10.1093/mnras/sts219)
- Meng, Y.-Z., Geng, J.-J., Zhang, B.-B., et al. 2018, *ApJ*, 860, 72, doi: [10.3847/1538-4357/aac2d9](https://doi.org/10.3847/1538-4357/aac2d9)
- Mészáros, P., & Rees, M. J. 2000, *ApJ*, 530, 292, doi: [10.1086/308371](https://doi.org/10.1086/308371)
- Paczynski, B. 1986, *ApJL*, 308, L43, doi: [10.1086/184740](https://doi.org/10.1086/184740)
- Pe'er, A. 2008, *ApJ*, 682, 463, doi: [10.1086/588136](https://doi.org/10.1086/588136)
- Pe'er, A., & Ryde, F. 2011, *ApJ*, 732, 49, doi: [10.1088/0004-637X/732/1/49](https://doi.org/10.1088/0004-637X/732/1/49)
- Pe'er, A., & Zhang, B. 2006, *ApJ*, 653, 454, doi: [10.1086/508681](https://doi.org/10.1086/508681)
- Pe'Er, A., Zhang, B.-B., Ryde, F., et al. 2012, *MNRAS*, 420, 468, doi: [10.1111/j.1365-2966.2011.20052.x](https://doi.org/10.1111/j.1365-2966.2011.20052.x)
- Piran, T., Shemi, A., & Narayan, R. 1993, *MNRAS*, 263, 861, doi: [10.1093/mnras/263.4.861](https://doi.org/10.1093/mnras/263.4.861)
- Preece, R. D., Briggs, M. S., Giblin, T. W., et al. 2002, *ApJ*, 581, 1248, doi: [10.1086/344252](https://doi.org/10.1086/344252)
- Rees, M. J., & Meszaros, P. 1994, *ApJL*, 430, L93, doi: [10.1086/187446](https://doi.org/10.1086/187446)
- Rees, M. J., & Mészáros, P. 2005, *ApJ*, 628, 847, doi: [10.1086/430818](https://doi.org/10.1086/430818)
- Ryde, F. 2004, *ApJ*, 614, 827, doi: [10.1086/423782](https://doi.org/10.1086/423782)
- . 2005, *ApJL*, 625, L95, doi: [10.1086/431239](https://doi.org/10.1086/431239)
- Sari, R., & Piran, T. 1997, *MNRAS*, 287, 110, doi: [10.1093/mnras/287.1.110](https://doi.org/10.1093/mnras/287.1.110)
- Shemi, A., & Piran, T. 1990, *ApJL*, 365, L55, doi: [10.1086/185887](https://doi.org/10.1086/185887)
- Tavani, M. 1996, *ApJ*, 466, 768, doi: [10.1086/177551](https://doi.org/10.1086/177551)
- Thompson, C. 1994, *MNRAS*, 270, 480, doi: [10.1093/mnras/270.3.480](https://doi.org/10.1093/mnras/270.3.480)
- Uhm, Z. L., & Zhang, B. 2014, *Nature Physics*, 10, 351, doi: [10.1038/nphys2932](https://doi.org/10.1038/nphys2932)
- Wang, Y., Xia, Z.-Q., Zheng, T.-C., Ren, J., & Fan, Y.-Z. 2023, *arXiv e-prints*, arXiv:2303.11083, doi: [10.48550/arXiv.2303.11083](https://doi.org/10.48550/arXiv.2303.11083)
- Wang, Y., Zheng, T.-C., & Jin, Z.-P. 2022, *ApJ*, 940, 142, doi: [10.3847/1538-4357/aca017](https://doi.org/10.3847/1538-4357/aca017)
- Yonetoku, D., Murakami, T., Nakamura, T., et al. 2004, *ApJ*, 609, 935, doi: [10.1086/421285](https://doi.org/10.1086/421285)
- Zhang, B., & Yan, H. 2011, *ApJ*, 726, 90, doi: [10.1088/0004-637X/726/2/90](https://doi.org/10.1088/0004-637X/726/2/90)
- Zhang, B.-B., Uhm, Z. L., Connaughton, V., Briggs, M. S., & Zhang, B. 2016, *ApJ*, 816, 72, doi: [10.3847/0004-637X/816/2/72](https://doi.org/10.3847/0004-637X/816/2/72)
- Zhang, H., Chen, X., & Böttcher, M. 2014, *ApJ*, 789, 66, doi: [10.1088/0004-637X/789/1/66](https://doi.org/10.1088/0004-637X/789/1/66)